ENGINEERING TRANSACTIONS • *Engng. Trans.* • **45**, 1, 5–28, 1997
Polish Academy of Sciences • Institute of Fundamental Technological Research

STRESS ANALYSIS IN THE EXTRUSION OF BIMETALLIC TUBES

J.L. ALCARAZ (BILBAO), J.M. MARTÍNEZ-ESNAOLA
and J. GIL-SEVILLANO (SAN SEBASTIÁN)

Stress analysis of the flow of a bimetallic tube in the process of extrusion through a conical die is presented in this paper. Two materials are involved in the process, one of them being of lower thickness and exhibiting finer properties than the other. The stress field is determined by assuming an axially-symmetric radial flow and material incompressibility, with no velocity discontinuity along the material interface and including friction between the bimetallic tube and the tools. Different extrusion conditions and different material combinations are compared to assess their influence on the stress levels in critical zones for the two possible locations of the finer material. It is concluded that the most influential parameters seem to be the yield stress ratio and the friction with the die.

NOTATION

$A, A_1, A_2, B, B_1, B_2,$ $C, C_0, K, \widehat{A}_1, \widehat{A}_2$	constants,
$\alpha_0, \alpha_1, \alpha_2$	mandrel, interface and die angles,
A_0, A_f	initial and final cross-sections,
C.R.A.	corrosion resistant alloy,
Δ	friction contribution parameter,
D_{ij}, σ_{ij}	strain rate and stress tensors,
f	void growth parameter,
F	piston force,
$h, \Psi, H, F_1, F_2, F_3$	functions of θ,
m	local friction factor,
m_0, m_2	friction coefficients with the mandrel and die,
r, φ, θ	spherical coordinates,
r_0, r_1	radial coordinates at the entry and exit sections,
R_0, R_f	outer radii at the entry and exit sections,
R_1	initial interface radius,
R_m	mandrel radius,
σ_h	hydrostatic stress,
u, v, w	velocity components,
Y, Y_1, Y_2	yield stresses (1 stands for inner, 2 for outer),
$\overline{\sigma}, \overline{\varepsilon}$	equivalent stress and strain,
$\overline{Y}$	mean yield stress.

1. Introduction

Bimetallic combinations are increasingly present in many different industrial applications. Here we are concerned with bimetallic tubes, used for example for oil conduits in sour wells. In such applications, as in many others, a good corrosion resistance, as well as a high mechanical strength, are required. Under these conditions, a bimetallic combination proves to be more economical than a monometallic tube of a corrosion-resistant alloy.

Bimetallic tubes are produced mostly in the well-known extrusion process. Much work has been devoted to the stress analysis of this process. One of the first attempts is the analysis of Shield [1], who considered radial flow of a single material through conical dies, and proposed a numerical solution for the equations governing the stress field. With the same type of analysis, Blazynski and Townley [2] analysed the process of plug drawing of bimetallic tubing in implosively welded composites under plane strain conditions. A mean strain hardening is also included. More recently, Durban [3] found a complete analytical solution following a Shield-type analysis and assuming small extrusion die angles. Durban applied also the results to a multilayered composite in the drawing and extrusion operations.

A different type of analysis is that of Atkins and Weinstein [4], who applied the force equilibrium approach to a bimetallic rod, assuming a rigid-plastic constitutive model. Later, Blazynski and Townley [2] extended the analysis of Atkins and Weinstein to strain-hardening conditions.

Other analyses [2, 5, 6, 7, 8] use the upper bound approach to determine the power required for the process. Moreover, the upper bound method has been used by others to introduce a failure condition in the bimetallic flow [9, 10, 11, 12]. The method, however, does not concentrate on the stress field within the working zone.

This paper is aimed at the stress determination during the flow of a bimetallic tube through a conical die. One of the two materials (the thinner layer) is referred to as the corrosion-resistant alloy and the other as the base steel. The analysis follows the initial steps of Durban's, but provides a more general solution valid for any die angles, and illustrates the influence of the different extrusion parameters on the stress field.

2. Axisymmetric stress field for a flowing material

Our aim in this section is to find a general expression for the stress field of a single material flowing radially with axial symmetry. Spherical coordinates (r, θ, φ) with origin in O are used, as shown in Fig. 1 a.

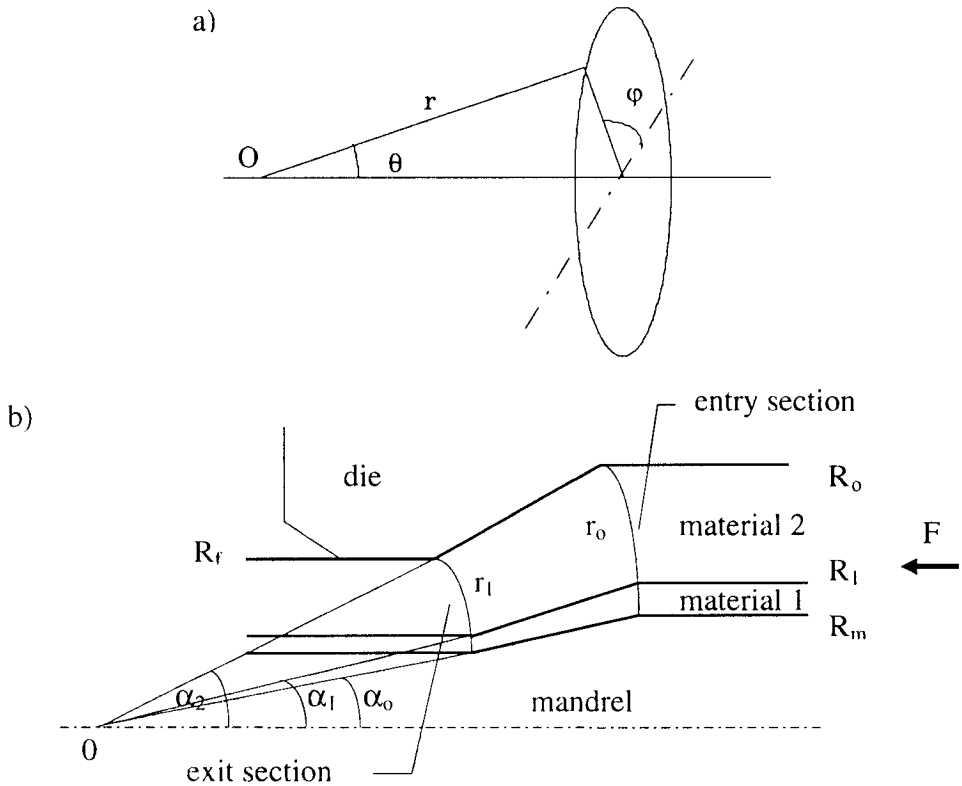

FIG. 1. a) Spherical coordinates used in the analysis, b) geometry of the process.

With the assumption of an axially-symmetric radial flow, the application of the condition of material incompressibility leads to the following velocity field:

$$u = -\frac{h(\theta)}{r^2} \qquad (v = w = 0), \tag{2.1}$$

where u stands for the radial velocity; v, w are the other two components, and $h(\theta)$ is an unknown function of the angular coordinate. The non-vanishing strain rate components, D_{ij}, easily deduced from (2.1), are $D_r = 2h/r^3$, $D_\theta = D_\varphi = -h/r^3$, $D_{r_\theta} = -h'/2r^3$.

The isotropic flow implies $\sigma_\varphi = \sigma_\theta$ and the axial symmetry implies $\tau_{r_\varphi} = \tau_{\varphi\theta} = 0$. Accordingly, the von Mises yield condition for a rigid-perfectly plastic behaviour leads to:

$$(\sigma_r - \sigma_\theta)^2 + 3\tau_{r\theta}^2 = Y^2, \tag{2.2}$$

where Y denotes the equivalent yield stress. Besides, the equations of the isotropic plastic flow provide:

$$\frac{\tau_{r\theta}}{\sigma_r - \sigma_\theta} = \frac{D_{r\theta}}{D_r - D_\theta} = \frac{-h'(\theta)}{6h(\theta)}. \tag{2.3}$$

Equation (2.2) can be written parametrically as:

$$\sigma_r - \sigma_\theta = Y\cos 2\Psi, \qquad \tau_{r\theta} = \frac{Y}{\sqrt{3}}\sin 2\Psi, \tag{2.4}$$

where Y is a parameter (depending on θ) that will be determined later.

From the radial and normal equilibrium equations, the following expressions are derived [1]:

$$2\left(\Psi' + \sqrt{3}\right)\cos 2\Psi + \operatorname{ctg}\theta \sin 2\Psi = \frac{2B\sqrt{3}}{Y}, \tag{2.5}$$

$$\left(H - \sqrt{3}\cos 2\Psi\right)' + 3\sin 2\Psi = 0, \tag{2.6}$$

where B is an integration constant, and Ψ, H are still unknown functions of θ. Moreover, the radial stress is expressed by:

$$\sigma_r = -2B\ln r + \frac{Y}{\sqrt{3}}H(\theta). \tag{2.7}$$

Now, it is convenient to define the local friction factor m as

$$m = \frac{\sqrt{3}|\tau_{r\theta}|}{Y} = |\sin 2\Psi| \tag{2.8}$$

according to $(2.4)_2$. In nearly uniform flow patterns, friction stresses are relatively small compared to the yield stress (i.e., $|\tau_{r\theta}| \ll Y$). Therefore, $|\Psi|$ becomes much smaller than unity. The integration of Eqs. (2.5) and (2.6) in this approach gives rise to the following expression for Ψ:

$$\Psi = \sqrt{3}\left(\frac{B}{Y} - 1\right)\operatorname{tg}\frac{\theta}{2} - \frac{\sqrt{3}K}{2Y\sin\theta}, \tag{2.9}$$

where K is an integration constant. Equation (2.9) coincides with that obtained by DURBAN [3], who proceeds with the analysis by assuming small die angles. Here no restrictions on the die angle are imposed.

From Eqs. (2.6) and (2.9), and with $|\Psi| \ll 1$, we obtain:

$$H' = -6\Psi = -6\sqrt{3}\left[\left(\frac{B}{Y} - 1\right)\operatorname{tg}\frac{\theta}{2} - \frac{K}{2Y\sin\theta}\right]. \tag{2.10}$$

Integration of (2.10) yields the following expression:

$$H = -6\sqrt{3}\left[-2\left(\frac{B}{Y} - 1\right)\ln\cos\frac{\theta}{2} - \frac{K}{2Y}\ln\operatorname{tg}\frac{\theta}{2}\right] + A\frac{\sqrt{3}}{Y}, \tag{2.11}$$

where A is a constant. Therefore, according to (2.7), (2.4), (2.11) and (2.9), the stress field is given by

$$
\begin{aligned}
\sigma_r &= -2B\ln r + \frac{Y}{\sqrt{3}}F = A - 2B\ln r + 12(B-Y)\ln\cos\frac{\theta}{2} + 3K\ln\operatorname{tg}\frac{\theta}{2}, \\
\sigma_\theta &= \sigma_r - Y\cos 2\Psi \approx \sigma_r - Y, \\
\tau_{r\theta} &= \frac{Y\sin 2\Psi}{\sqrt{3}} \approx \frac{2Y}{\sqrt{3}}\Psi = 2(B-Y)\operatorname{tg}\frac{\theta}{2} - \frac{K}{\sin\theta}.
\end{aligned}
\tag{2.12}
$$

The associated velocity profile is determined by (2.1), where $h(\theta)$ is a function satisfying the condition

$$
\frac{\sqrt{3}}{6}\frac{h'}{h} = -2\sqrt{3}\left[\left(\frac{B}{Y}-1\right)\operatorname{tg}\frac{\theta}{2} - \frac{K}{2Y\sin\theta}\right]. \tag{2.13}
$$

After integration of (2.13), we obtain

$$
\begin{aligned}
h &= C_0\exp\left[24\left(\frac{B}{Y}-1\right)\ln\cos\frac{\theta}{2} + \frac{6K}{Y}\ln\operatorname{tg}\frac{\theta}{2}\right] \\
&= C_0\left[\left(\cos\frac{\theta}{2}\right)^{24\left(\frac{B}{Y}-1\right)}\left(\operatorname{tg}\frac{\theta}{2}\right)^{\frac{6K}{Y}}\right],
\end{aligned}
\tag{2.14}
$$

where C_0 is a constant.

Once the stress field and the velocity profile are known, only constants in (2.12) and (2.14) remain to be determined from the corresponding boundary conditions.

3. Solution for a bimetallic tube

The stress field derived in the previous section will be used for the stress determination in the bimetallic combination. This implies that the flow is spherical and perfectly radial. Consequently, no velocity discontinuity can arise along the material interface. This is evidently an ideal case, not always attainable in real extrusion processes where the material heterogeneity is likely to prevent a perfectly compatible flow.

Figure 1 b shows the geometry of the process. A tube composed of two materials is forced against a rigid conical die flowing over a fixed mandrel. In the notation that follows, subscript 1 will refer to the inner material and subscript 2 to the outer one. Moreover, the thinner layer corresponds to the corrosion-resistant alloy and the other to the low-alloyed or base steel.

To obtain the stress solution in the bimetallic tube, the constants in Eq. (2.12) for each material must be determined. In other words, we must impose the continuity and boundary conditions.

Firstly, the normal and shear stresses are continuous across the material interface. Using $(2.12)_1$, the continuity of the normal stress leads to

$$(3.1)\qquad -2B_1 \ln r + A_1 + 12(B_1 - Y_1)\ln\cos\frac{\alpha_1}{2} + 3K_1 \ln \operatorname{tg}\frac{\alpha_1}{2} - Y_1 = -2B_2 \ln r + A_2 + 12(B_2 - Y_2)\ln\cos\frac{\alpha_1}{2} + 3K_2 \ln \operatorname{tg}\frac{\alpha_1}{2} - Y_2$$

and the condition of continuity of the shear stress $(2.12)_3$ leads to

$$(3.2)\qquad 2(B_1 - Y_1)\operatorname{tg}\frac{\alpha_1}{2} - \frac{K_1}{\sin\alpha_1} = 2(B_2 - Y_2)\operatorname{tg}\frac{\alpha_1}{2} - \frac{K_2}{\sin\alpha_1}.$$

It is interesting to note that Eq. (3.2) implies $B_1 = B_2 = B$.

Secondly, two boundary conditions for friction between the tube and the mandrel and the die are considered. By assuming the friction model given by (2.8) and constant friction coefficients, m_0 with the mandrel (at $\theta = \alpha_0$) and m_2 with the die (at $\theta = \alpha_2$), the following two equations are obtained:

$$(3.3)\qquad 2(B_1 - Y_1)\operatorname{tg}\frac{\alpha_0}{2} - \frac{K_1}{\sin\alpha_0} = -\frac{m_0 Y_1}{\sqrt{3}},$$

$$(3.4)\qquad 2(B_2 - Y_2)\operatorname{tg}\frac{\alpha_2}{2} - \frac{K_2}{\sin\alpha_2} = \frac{m_2 Y_2}{\sqrt{3}}.$$

Note that the friction with the mandrel provides a negative shear stress. Accordingly, a minus sign appears in (3.3).

Finally, on the basis of a pure extrusion process, the axial component of the total force at the die exit should vanish. Using this boundary condition, the following expression is obtained:

$$(3.5)\qquad 0 = \int_{\alpha_0}^{\alpha_1} \sigma_r^{(1)}\Big|_{r_1} \cos\theta\sin\theta\,d\theta + \int_{\alpha_1}^{\alpha_2} \sigma_r^{(2)}\Big|_{r_1} \cos\theta\sin\theta\,d\theta - \int_{\alpha_0}^{\alpha_1} \tau_{r\theta}\sin^2\theta\,d\theta - \int_{\alpha_1}^{\alpha_2} \tau_{r\theta}\sin^2\theta\,d\theta = (-2B\ln r_1 + A_1)\left(\sin^2\alpha_1 - \sin^2\alpha_0\right)/2 + 12(B - Y_1)\left[F_1(\alpha_1) - F_1(\alpha_0)\right] + 3K_1\left[F_2(\alpha_1) - F_2(\alpha_0)\right] + (-2B\ln r_1 + A_2)\left(\sin^2\alpha_2 - \sin^2\alpha_1\right)/2 + 12(B - Y_2)\left[F_1(\alpha_2) - F_1(\alpha_1)\right] + 3K_2\left[F_2(\alpha_2) - F_2(\alpha_1)\right] - 2(B - Y_1)\left[F_3(\alpha_1) - F_3(\alpha_0)\right] - 2(B - Y_2)\left[F_3(\alpha_2) - F_3(\alpha_1)\right] + K_1(\cos\alpha_0 - \cos\alpha_1) + K_2(\cos\alpha_1 - \cos\alpha_2),$$

where the functions F_1, F_2 and F_3 are defined as:

$$F_1(\theta) = \int \ln\cos\frac{\theta}{2}\cos\theta\sin\theta\,d\theta = \frac{1}{2}\sin^2\theta\ln\cos\frac{\theta}{2} + \frac{1}{2}\cos^4\frac{\theta}{2} - \cos^2\frac{\theta}{2},$$

$$F_2(\theta) = \int \ln \operatorname{tg} \frac{\theta}{2} \cos\theta \sin\theta \, d\theta = \frac{1}{2} \sin^2\theta \ln \operatorname{tg} \frac{\theta}{2} + \cos^2 \frac{\theta}{2},$$

$$F_3(\theta) = \int \operatorname{tg} \frac{\theta}{2} \sin^2\theta \, d\theta = 2 \sin^4 \frac{\theta}{2}.$$

At this point, we have a system of five equations, (3.1) to (3.5), for five constants, K_1, K_2, B, A_1, A_2. Solving this system we obtain

$$K_1 = \sin\alpha_0 \left[2(B - Y_1) \operatorname{tg} \frac{\alpha_0}{2} + \frac{m_0 Y_1}{\sqrt{3}} \right],$$

$$K_2 = \sin\alpha_2 \left[2(B - Y_2) \operatorname{tg} \frac{\alpha_2}{2} - \frac{m_2 Y_2}{\sqrt{3}} \right],$$

$$B = \frac{Y_2 \sin^2 \frac{\alpha_2}{2} - Y_1 \sin^2 \frac{\alpha_0}{2} + \frac{m_2 Y_2}{4\sqrt{3}} \sin\alpha_2 + \frac{m_0 Y_1}{4\sqrt{3}} \sin\alpha_0 + (Y_1 - Y_2) \sin^2 \frac{\alpha_1}{2}}{\sin^2 \frac{\alpha_2}{2} - \sin^2 \frac{\alpha_0}{2}}$$

$$= \overline{Y} + \Delta,$$

$$A_1 = Y_1 + 12 Y_1 \left(\ln \cos \frac{\alpha_1}{2} + \sin^2 \frac{\alpha_1}{2} \ln \operatorname{tg} \frac{\alpha_1}{2} \right) + C, \tag{3.6}$$

$$A_2 = Y_2 + 12 Y_2 \left(\ln \cos \frac{\alpha_1}{2} + \sin^2 \frac{\alpha_1}{2} \ln \operatorname{tg} \frac{\alpha_1}{2} \right) + C, \tag{3.7}$$

with the mean yield stress being defined as

$$\overline{Y} = \frac{Y_2 \left(\sin^2 \frac{\alpha_2}{2} - \sin^2 \frac{\alpha_1}{2} \right) + Y_1 \left(\sin^2 \frac{\alpha_1}{2} - \sin^2 \frac{\alpha_0}{2} \right)}{\sin^2 \frac{\alpha_2}{2} - \sin^2 \frac{\alpha_0}{2}}.$$

The contribution of friction is determined by the parameter

$$\Delta = \frac{\frac{m_2 Y_2}{4\sqrt{3}} \sin\alpha_2 + \frac{m_0 Y_1}{4\sqrt{3}} \sin\alpha_0}{\sin^2 \frac{\alpha_2}{2} - \sin^2 \frac{\alpha_0}{2}},$$

and constant C in Eqs. (3.6) and (3.7) follows from (3.5) as

$$\begin{aligned} C = \frac{-2}{\sin^2\alpha_2 - \sin^2\alpha_0} \Big[& \left(-2B \ln r_1 + \hat{A}_1 \right) \left(\sin^2\alpha_1 - \sin^2\alpha_0 \right) \\ & + 12(B - Y_1) \left[F_1(\alpha_1) - F_1(\alpha_0) \right] + 3K_1 \left[F_2(\alpha_1) - F_2(\alpha_0) \right] \\ & + \left(-2B \ln r_1 + \hat{A}_2 \right) \left(\sin^2\alpha_2 - \sin^2\alpha_1 \right) + 12(B - Y_2) \left[F_1(\alpha_2) - F_1(\alpha_1) \right] \\ & + 3K_2 \left[F_2(\alpha_2) - F_2(\alpha_1) \right] - 2(B - Y_1) \left[F_3(\alpha_1) - F_3(\alpha_0) \right] \\ & - 2(B - Y_2) \left[F_3(\alpha_2) - F_3(\alpha_1) \right] + K_1(\cos\alpha_0 - \cos\alpha_1) + K_2(\cos\alpha_1 - \cos\alpha_2) \Big], \end{aligned}$$

where we have denoted

$$\hat{A}_1 = A_1 - C, \qquad \hat{A}_2 = A_2 - C.$$

Therefore, the stress field for a bimetallic tube can be written as:

$$\begin{aligned}
\sigma_{r_1} &= -2\left(\overline{Y} + \Delta\right)\ln r + 12Y_1\left(\ln\cos\frac{\alpha_1}{2} + \sin^2\frac{\alpha_1}{2}\ln\operatorname{tg}\frac{\alpha_1}{2}\right) \\
&\quad + 12\left(\overline{Y} + \Delta - Y_1\right)\ln\cos\frac{\theta}{2} + 12\left(\overline{Y} + \Delta - Y_1\right)\sin^2\frac{\alpha_0}{2}\ln\operatorname{tg}\frac{\theta}{2} \\
&\quad + \sqrt{3}m_0Y_1\sin\alpha_0\ln\operatorname{tg}\frac{\theta}{2} + C + Y_1\,, \qquad (3.8)\\
\sigma_{\theta_1} &= \sigma_{r_1} - Y_1\,, \\
\tau_{r\theta_1} &= 2\left(\overline{Y} + \Delta - Y_1\right)\operatorname{tg}\frac{\theta}{2} - \frac{4\left(\overline{Y} + \Delta - Y_1\right)\sin^2\dfrac{\alpha_0}{2} + \dfrac{m_0Y_1\sin\alpha_0}{\sqrt{3}}}{\sin\theta}
\end{aligned}$$

for Material 1, and

$$\begin{aligned}
\sigma_{r_2} &= -2\left(\overline{Y} + \Delta\right)\ln r + 12Y_2\left(\ln\cos\frac{\alpha_1}{2} + \sin^2\frac{\alpha_1}{2}\ln\operatorname{tg}\frac{\alpha_1}{2}\right) \\
&\quad + 12\left(\overline{Y} + \Delta - Y_2\right)\ln\cos\frac{\theta}{2} + 12\left(\overline{Y} + \Delta - Y_2\right)\sin^2\frac{\alpha_2}{2}\ln\operatorname{tg}\frac{\theta}{2} \\
&\quad - \sqrt{3}m_2Y_2\sin\alpha_2\ln\operatorname{tg}\frac{\theta}{2} + C + Y_2\,, \qquad (3.9)\\
\sigma_{\theta_2} &= \sigma_{r_2} - Y_2\,, \\
\tau_{r\theta_2} &= 2\left(\overline{Y} + \Delta - Y_2\right)\operatorname{tg}\frac{\theta}{2} - \frac{4\left(\overline{Y} + \Delta - Y_2\right)\sin^2\dfrac{\alpha_2}{2} - \dfrac{m_2Y_2\sin\alpha_2}{\sqrt{3}}}{\sin\theta}
\end{aligned}$$

for Material 2. For small die angles, Eqs. (3.8) and (3.9) reduce to the solution given by DURBAN [3].

Finally, the total force required for the process may be estimated by the integration of forces in the axial direction, x : $F = \int \sigma_x\, dS$, where $dS = 2\pi r_0^2 \sin\theta\, d\theta$ is a surface element in spherical coordinates, and the axial stress is $\sigma_x = \sigma_r\cos\theta - \tau_{r\theta}\sin\theta$. From this calculation, we obtain

$$\begin{aligned}
&2\pi r_0^2\int_{\alpha_0}^{\alpha_1}\sigma_r^{(1)}\Big|_{r_0}\cos\theta\sin\theta\, d\theta + \int_{\alpha_1}^{\alpha_2}\sigma_r^{(2)}\Big|_{r_0}\cos\theta\sin\theta\, d\theta - \int_{\alpha_0}^{\alpha_1}\tau_{r\theta}\sin^2\theta\, d\theta \\
&\qquad - \int_{\alpha_1}^{\alpha_2}\tau_{r\theta}\sin^2\theta\, d\theta = 2\pi r_0^2\left(-B\ln\frac{r_0}{r_1}\right)\left(\sin^2\alpha_2 - \sin^2\alpha_0\right).
\end{aligned} \qquad (3.10)$$

4. Results

In this section, Eqs. (3.8) and (3.9) will be applied to different geometries, materials and extrusion conditions. To illustrate the behaviour of the stress solution, let us first consider a particular case for each of the two possible locations of the corrosion-resistant alloy (C.R.A.), acting as the inner or outer layer. The data in both cases are taken from an actual process used in Tubacex (Llodio, Spain). In the notation, we refer to σ_r, σ_θ and $\tau_{r\theta}$ as the radial, normal and shear stress, respectively.

4.1. Application to Inconel 625 and AISI 4130

4.1.1. Inner C.R.A. location. Let us start with the case of an inner C.R.A. location. The initial tube exhibits an inner/outer thickness ratio of 1/5 and an inner/outer yield stress ratio of 2.2. The remaining dimensions and parameters are included in Table 1.

Table 1. Normalized reference values for both locations of the C.R.A. layer. R_0 and R_f stand for the outer radius at the entry and exit sections, respectively; R_1 for the initial interface radius; R_m for the mandrel radius; m_0 and m_2 for the friction coefficient with the mandrel and die, respectively, and α_0, α_1, α_2 for the mandrel, interface and die angle, respectively.

Case	Y_1/Y_2	α_0	α_1	α_2	R_1/R_0	R_m/R_0	R_f/R_0	m_0	m_2
inner C.R.A.	2.2	9.15°	12.5°	30°	0.436	0.32	0.73	0.1	0.15
outer C.R.A.	1/2.2	9.15°	24.3°	30°	0.884	0.32	0.73	0.1	0.15

The aplication of Eqs. (3.8) and (3.9) provide the stress distributions plotted in Fig. 2, after being normalized with respect to the yield stress of the base steel (AISI 4130). Figure 2 a shows the radial stress at $\theta = \alpha_0$, α_1 and α_2, as a function of the radial coordinate, and Fig. 2 b displays the radial stress at $r = r_0$ and r_1 (i.e., the entry and exit surfaces, respectively), as a function of the angular coordinate, θ. According to the von Mises model for a rigid-plastic material, a discontinuity of value $Y_1 - Y_2$ across the interface is obtained. A small dependence on the θ angle can also be noticed in both Figs. 2 a and 2 b. The highest values of the radial stress occur in the harder material. Furthermore, these values increase on approaching the die exit. The sign of the radial stress in the outer material changes during the process, remaining positive at the exit. The inner material, however, remains always tensile. These residual stresses prove to be important if they are positive, because they could induce some decohesion in the final product.

The normal stress is plotted in Figs. 2 c – d for the same values of θ and r as in Figs. 2 a – b. It can be seen from Fig. 2 c, that this stress component is continuous

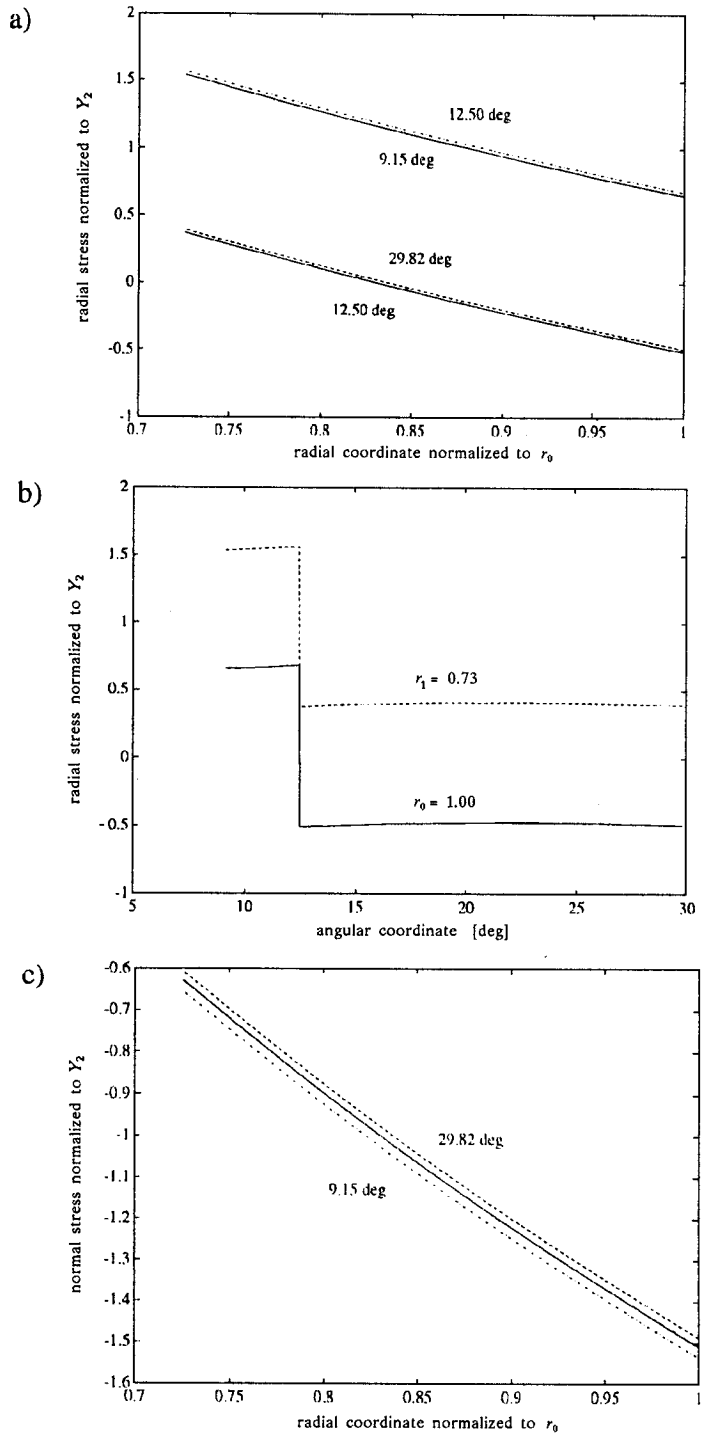
a)
radial stress normalized to Y_2
12.50 deg
9.15 deg
29.82 deg
12.50 deg
radial coordinate normalized to r_0
b)
radial stress normalized to Y_2
r_1 = 0.73
r_0 = 1.00
angular coordinate [deg]
c)
normal stress normalized to Y_2
29.82 deg
9.15 deg
radial coordinate normalized to r_0

[FIG. 2]

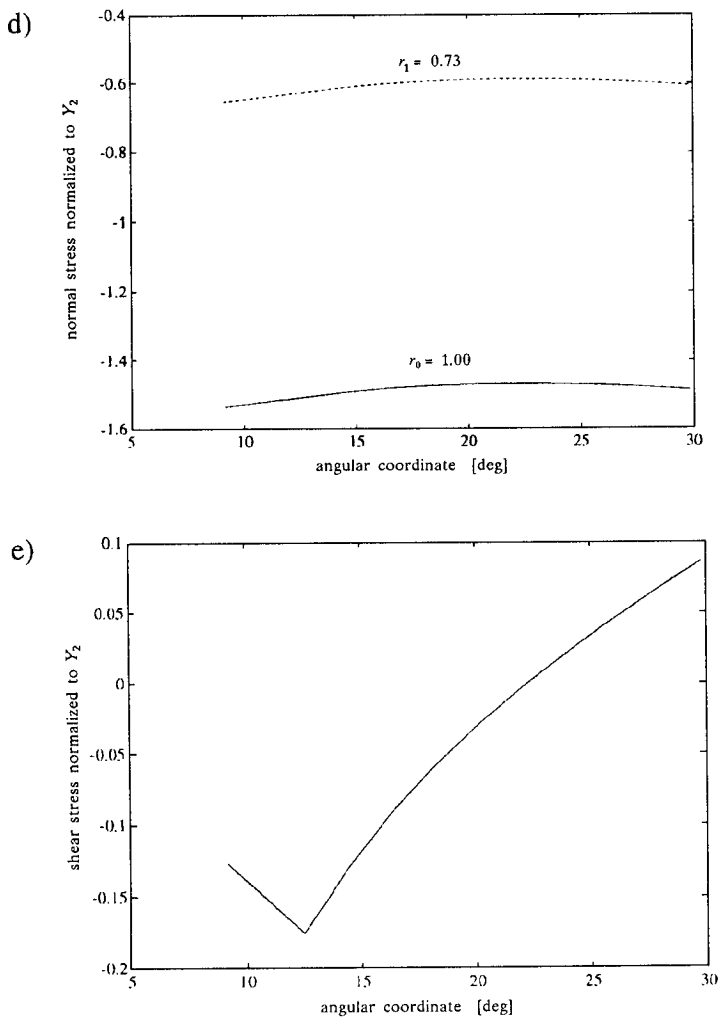

FIG. 2. Normalized stresses for the inner C.R.A. case: a) radial stress at α_0, α_1 and α_2, b) radial stress at r_0 and r_1, c) normal stress at α_0, α_1 and α_2, d) normal stress at r_0 and r_1, e) shear stress. $\alpha_0 = 9.15°$, $\alpha_1 = 12.5°$, $\alpha_2 = 30°$, $r_0 = 0.346$ m and $r_1 = 0.251$ m.

across the interface and takes negative values in both materials. Figure 2 d shows that the influence of θ is also negligible. The module of this stress component in the inner layer (the harder material) is higher than in the outer layer and decreases upon approaching the exit (cf. Fig. 2 c).

Finally, Fig. 2 e shows the shear stress as a function of θ. According to $(2.12)_3$, this stress component does not depend on the radial coordinate. Figure 2 e also shows that the maximum absolute value is attained at the interface (as also pointed out by PAWELSKI and RASP, [13]). The shear stress is negative at the interface and its absolute value decreases at farther locations. The outer material

being thicker, the sign changes even within this material. The order of magnitude of the shear stress is lower than that of the two other stresses.

4.1.2. Outer C.R.A. location. Consider now the opposite situation, with the C.R.A. layer placed outside (i.e., a combination AISI 4130/Inconel 625). In this case, the inner/outer thickness ratio of the tube is 5 and the inner/outer yield stress ratio is 1/2.2. Other parameters can be found in Table 1.

Similarly to Fig. 2, the stress distributions are depicted in Fig. 3. They are again referred to the yield stress of the base steel. As shown in Figs. 3 a – b, the radial stresses are higher in the C.R.A. layer than in the other, what happened in the case of an inner C.R.A. (although the maximum value is now a little higher). Likewise, from Figs. 3 c – d normal stresses in the C.R.A. material are obtained higher in module than in the base steel, as in Figs. 2 c – d. Finally, the shear stress shown in Fig. 3 e has an opposite sign in the harder material and its magnitude is almost doubled, as compared to Fig. 2 e. Note that the stress levels in Fig. 3 are higher than in Fig. 2, because the material interface flows closer to the die.

4.2. Influence of the extrusion parameters

In this section, we proceed with a systematic analysis of the influence of the different parameters involved in Eqs. (3.8) and (3.9). As before, the two cases (with outer and inner C.R.A.) will be clearly distinguished. The reference values for the two locations are the same as those given in Table 1.

To establish an appropriate comparison between the different cases, some characteristic values are selected. According to Figs. 2 and 3, and as experience confirms, the interfacial point at the die exit provides the most dangerous stress state. Therefore, stresses at this location are selected. Note that two sets of values can be obtained: one in each material. These values will be again normalized with respect to the yield stress of the common steel alloy.

4.2.1. Inner C.R.A. location. The results of the stress components for an inner C.R.A. location are plotted in Figs. 4 a – f. In this case, the stresses are computed in the inner interface element, which provides higher levels than the outer one.

Figure 4a shows the influence of the yield stress ratio (Y_1/Y_2). It can be noticed that as this ratio increases, all the stresses also increase, because of the higher yield stress of the harder material and the more critical heterogeneity at the interface. The radial stress reaches the highest values and is subject to considerable variation. Compared to the remaining parameters, the yield stress ratio becomes one of the most influential variables.

a)

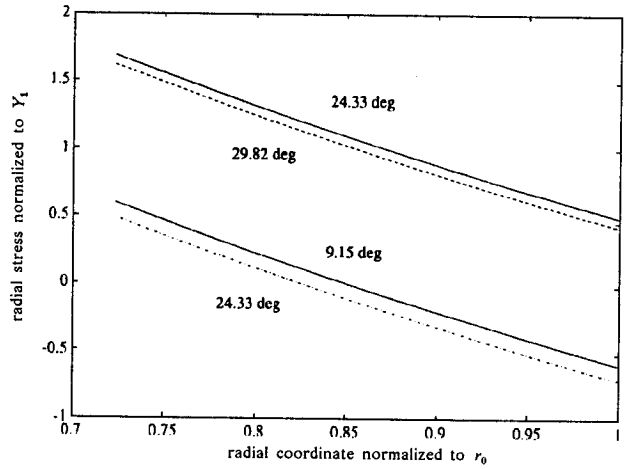
radial stress normalized to Y_1
radial coordinate normalized to r_0
24.33 deg
29.82 deg
9.15 deg
24.33 deg

b)

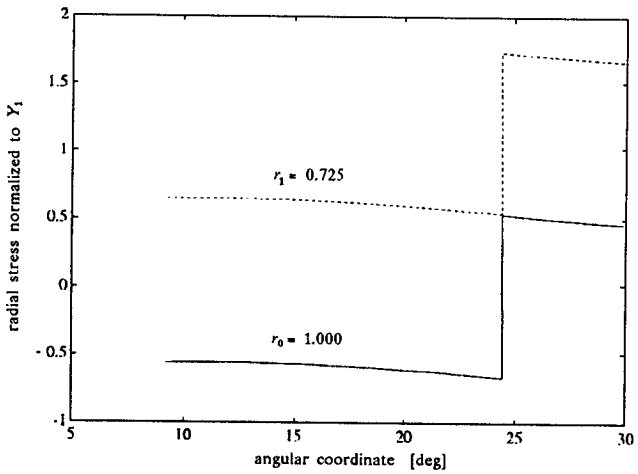
radial stress normalized to Y_1
angular coordinate [deg]
r_1 = 0.725
r_0 = 1.000

c)

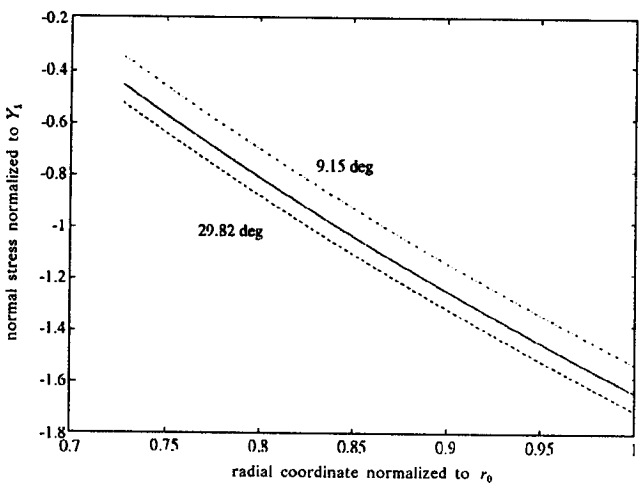
normal stress normalized to Y_1
radial coordinate normalized to r_0
9.15 deg
29.82 deg

[FIG. 3]

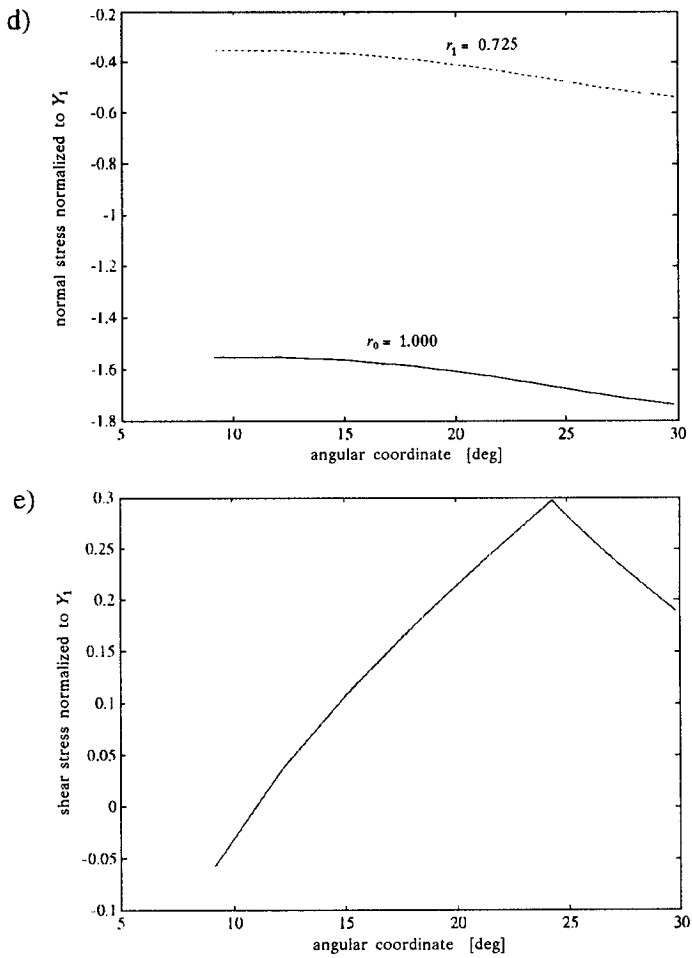

FIG. 3. Normalized stresses for the outer C.R.A. case: a) radial stress at α_0, α_1 and α_2, b) radial stress at r_0 and r_1, c) normal stress at α_0, α_1 and α_2, d) normal stress at r_0 and r_1, e) shear stress. $\alpha_0 = 9.15°$, $\alpha_1 = 24.3°$, $\alpha_2 = 30°$, $r_0 = 0.346$ m and $r_1 = 0.251$ m.

In Fig. 4b, the effect of the die angle is illustrated. With larger angles, the shear and normal stresses increase, while the radial stress diminishes. The explanation of this behaviour is that a greater die angle makes the stresses "more compressive".

The effect of the interface radius is shown in Fig. 4 c. An increase in this magnitude produces similar effects as the increase in the die angle, i.e., the absolute value of negative stress components (especially the normal stress) increases and the radial stress decreases. Two reasons could be given to understand this behaviour. Firstly, the stresses are more compressive when the interface approaches the die. And besides, a higher interface radius makes the thickness of the harder material (inner location) greater.

a)

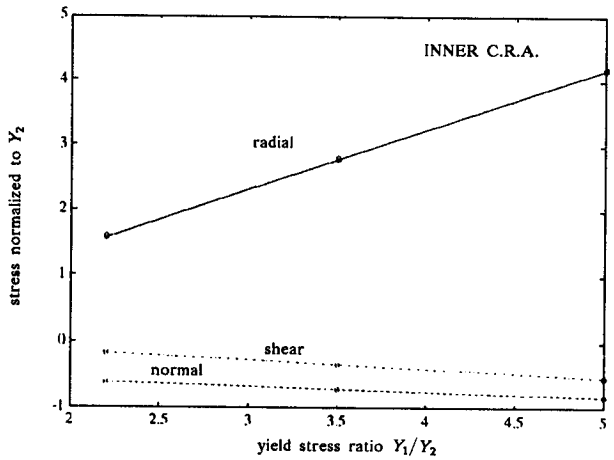
INNER C.R.A.
radial
shear
normal
stress normalized to Y_2
yield stress ratio Y_1/Y_2
5
4
3
2
1
0
-1
2
2.5
3
3.5
4
4.5
5

b)

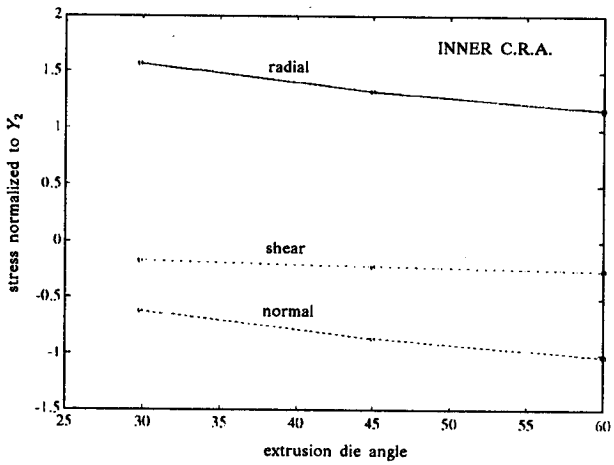
INNER C.R.A.
radial
shear
normal
stress normalized to Y_2
extrusion die angle
2
1.5
1
0.5
0
-0.5
-1
-1.5
25
30
35
40
45
50
55
60

c)

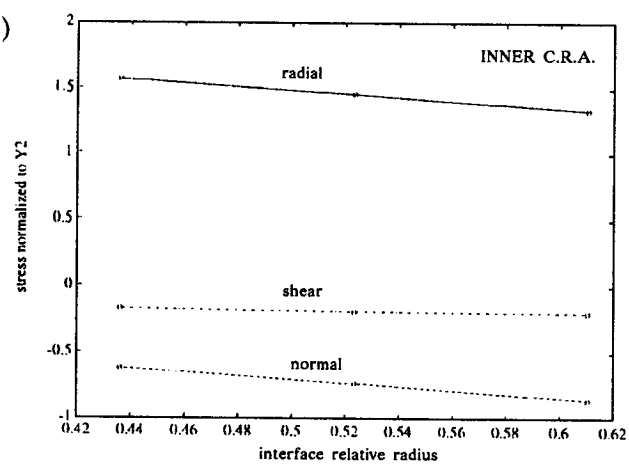
INNER C.R.A.
radial
shear
normal
stress normalized to Y2
interface relative radius
2
1.5
1
0.5
0
-0.5
-1
0.42
0.44
0.46
0.48
0.5
0.52
0.54
0.56
0.58
0.6
0.62

[FIG. 4]

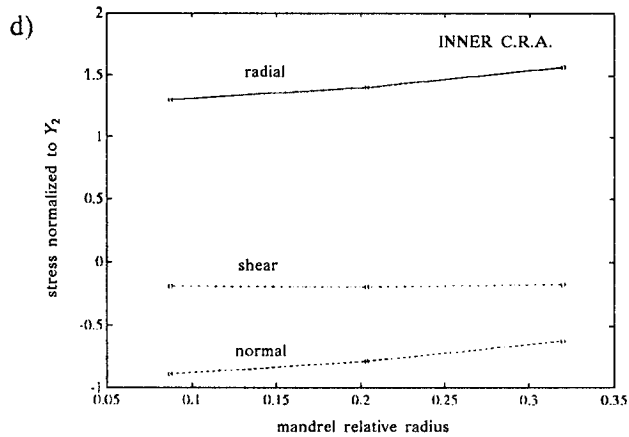

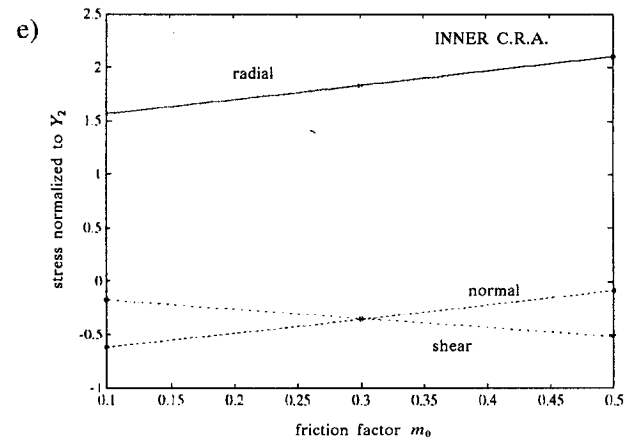

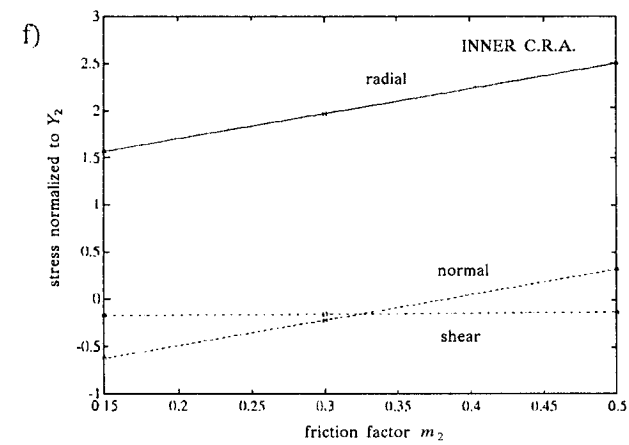

FIG. 4. Influence of the extrusion parameters on the stress levels at the interfacial exit point for the inner C.R.A. case: a) yield stress ratio, b) extrusion die angle, c) relative interface radius, d) relative mandrel radius, e) friction coefficient with the mandrel, f) friction coefficient with the die.

The results of the influence of the mandrel size are shown in Fig. 4 d. The effect of an increase in this parameter is opposite to that of an increase in the interface radius, because with larger mandrels, the thickness of the inner harder material decreases. In particular, we obtain higher radial stresses, lower normal stresses and almost identical shear stresses.

It has been verified that the final size of the tube (or, equivalently, the extrusion ratio) has no influence on the stress levels. Although this result could be surprising, it follows naturally from the consideration of a spherical radial flow and vanishing of the resulting axial stress at the die exit section (see (3.5)).

The effects of the friction coefficients (m_0 and m_2) are plotted in Figs. 4 e and f, respectively. The friction with the mandrel slows down the flow of the inner, harder material. For this reason, Fig. 4 e shows that the positive radial stress increases and the shear stress becomes more negative as m_0 increases. There is also a tensile effect on the normal component. On the other hand, Fig. 4 f shows that the friction with the die makes the radial stress increase, since it involves a hindrance to the flow. On the other hand, the shear stress becomes "less negative", although this influence is small due to a larger distance from the die. A tensile effect of an increasing m_2 coefficient on the normal stress is also observed.

4.2.2. Outer C.R.A. location. In the case of a tube with an outer C.R.A. location, stresses at the interface point in the outer material are plotted in Figs. 5 a–f. As the outer layer is now extruded with more difficulty, shear stresses assume positive values in the C.R.A. and a change of sign takes place in the base steel. Normal stresses remain negative.

The influence of the yield stress ratio Y_1/Y_2 is shown in Fig. 5 a. As expected, the shear and radial stresses increase with that ratio, due to a higher C.R.A. yield stress combined with a stronger discrepancy in the plastic flow. The normal stress slightly decreases in module as the yield stress ratio increases.

Figure 5b illustrates the effect of the die angle. At greater angles, the radial and normal stresses become more compressive (as in Fig. 4 b) and the shear stress increases. The latter effect is attributed to the fact that larger die angles involve more flow disturbance in the outer layer, thus making the shear component at the interface increase.

The influence of the interface radius, shown in Fig. 5 c, differs from the inner C.R.A. case. The absolute value of normal stress decreases with the increase in the interface radius, because of the corresponding decrease in the thickness of the outer layer (the C.R.A.). On the other hand, as the interface approaches the die, the shear stress slightly increases and the radial stress also increases due to the more favourable geometric conditions for the inner material to flow and, consequently, the more pronounced effect of the inner material on the outer one.

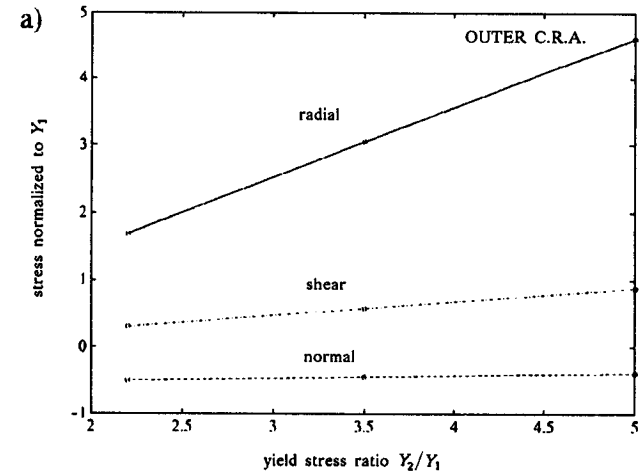
a)
OUTER C.R.A.
radial
shear
normal
stress normalized to Y_1
yield stress ratio Y_2/Y_1
5
4
3
2
1
0
-1
2
2.5
3
3.5
4
4.5
5

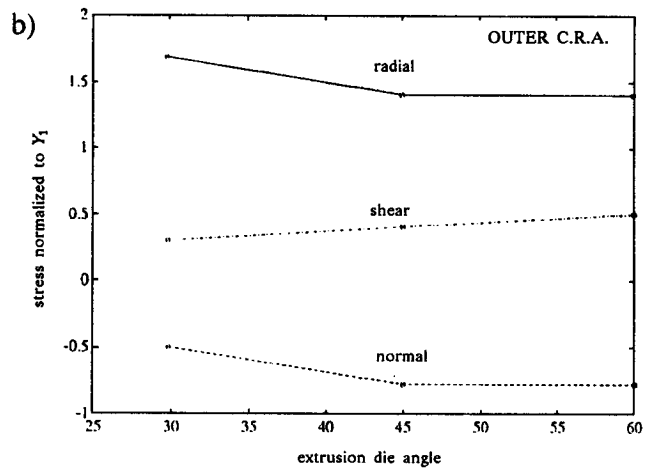
b)
OUTER C.R.A.
radial
shear
normal
stress normalized to Y_1
extrusion die angle
2
1.5
1
0.5
0
-0.5
-1
25
30
35
40
45
50
55
60

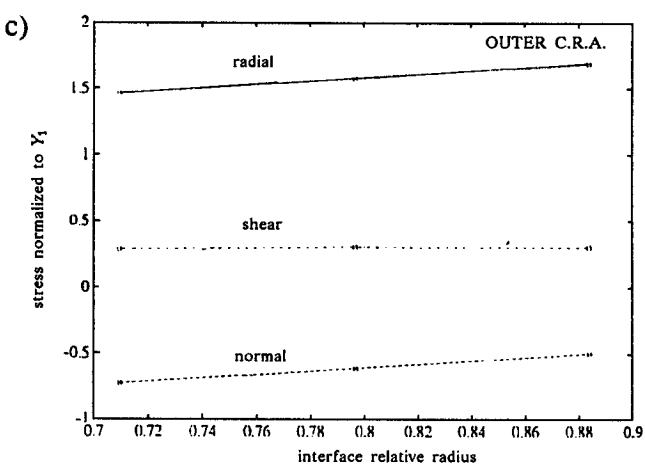
c)
OUTER C.R.A.
radial
shear
normal
stress normalized to Y_1
interface relative radius
2
1.5
1
0.5
0
-0.5
-1
0.7
0.72
0.74
0.76
0.78
0.8
0.82
0.84
0.86
0.88
0.9

[FIG. 5]

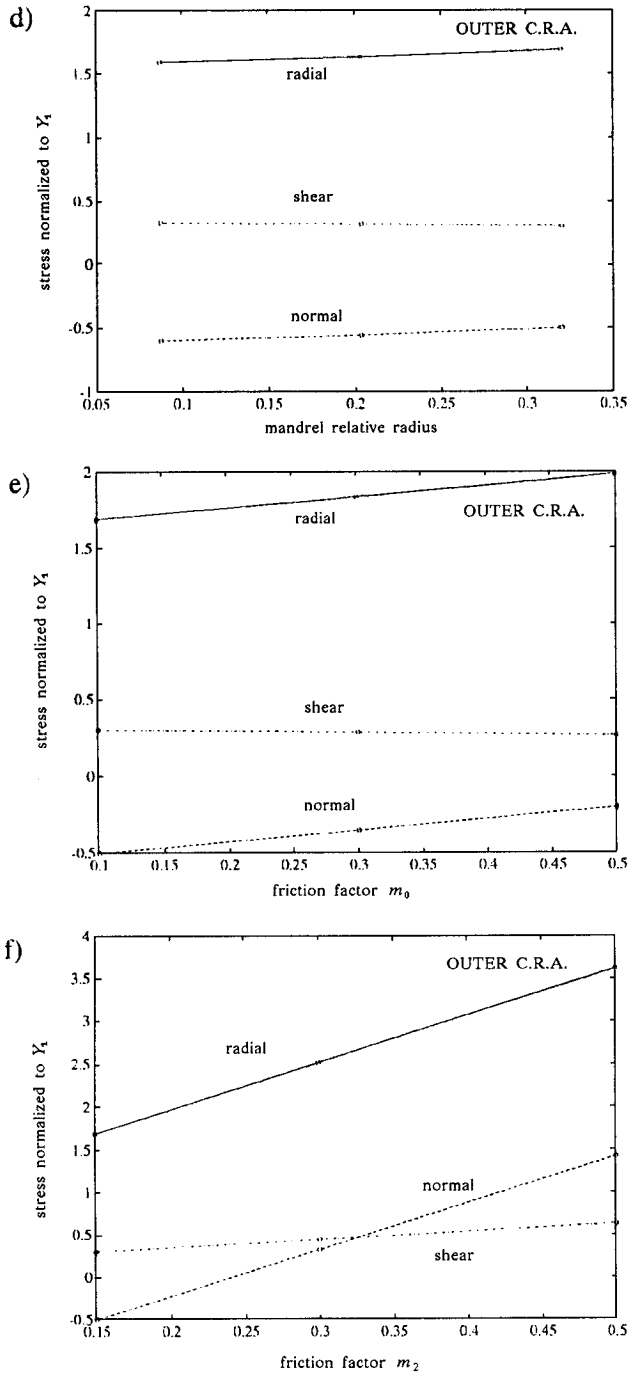

FIG. 5. Influence of the extrusion parameters on the stress levels at the interfacial exit point for the outer C.R.A. case: a) yield stress ratio, b) extrusion die angle, c) relative interface radius, d) relative mandrel radius, e) friction coefficient with the mandrel, f) friction coefficient with the die.

The tensile effect of the inner material affects the variation of both the normal and radial stresses.

By assuming several mandrel sizes, Fig. 5 d is obtained. It can be seen that on increasing the relative size of the mandrel, only small stress variations are derived: a lower normal stress, a lower shear stress and a higher radial stress. Since the increase in the mandrel size implies the decrease in the inner material thickness, the effect of the yield discrepancy between the layers turns out to be reduced. This leads to a decrease in the normal and shear stresses at the interface. The radial stress, however, increases because the inner yielding is facilitated by a larger mandrel.

Finally, the variations in stress with the friction coefficients m_0 and m_2 are plotted in Figs. 5 e and f, respectively. Similarly to the inner C.R.A. case, an increase in both friction coefficients involves a tensile effect on the normal stress and a higher radial component (because this component opposes the flow). However, the shear stress, being now positive (i.e., in the sense of the flow), decreases slightly with the mandrel friction and increases with the die friction. As shown in Fig. 5 e, the effects of an increase in the mandrel friction are similar to and more pronounced than those of an increase in the mandrel size. The flow of the softer material is impeded by the mandrel friction, giving rise to lower shear stresses and also lower absolute values of normal stresses at the interface. On the other hand, an increase in the die friction (Fig. 5 f) prevents the flow of the outer, leading to an increase in the shear and radial stresses. For coefficients higher than 0.25, it is also noticed in Fig. 5 f that there is a change of sign in the normal stress, due to the proximity of the interface to the die.

5. Ductile failure

Up to now stress fields have been derived and the influence of the extrusion parameters on the maximum stress at the interface has been determined. In this section, a ductile failure criterium will be established so as to assess the most critical conditions and variables in the process.

Let the *void growth parameter* f be defined as:

$$f = \int_0^{\bar{\varepsilon}} \exp\left(1.5\frac{\sigma_h}{\bar{\sigma}}\right) d\bar{\varepsilon}, \qquad \sigma_h > 0, \tag{5.1}$$

where $\bar{\sigma}$ and $\bar{\varepsilon}$ are the equivalent plastic stress and strain, respectively, and σ_h is the hydrostatic stress. According to (5.1), this parameter represents an accumulated plastic strain corrected by the hydrostatic stress and will be considered here as an indication of ductile failure. It is based on a factor deduced by Rice

and TRACEY [14]. The fracture condition will be locally fulfilled when a critical value of f is attained.

The results of evaluation of the parameter f, normalized with respect to the uniform equivalent strain ($\ln A_0/A_f$, where A_0 and A_f are, respectively, the initial and final cross-section of the tube), are given in Tables 2 and 3. In the case of an inner C.R.A. location (Table 2), the most important variations take place for the friction coefficients, m_0 and m_2. On using high friction coefficients, the normal stress at the exit point of the interface decreases considerably, assuming even positive values. Another relevant variable is the yield stress ratio, Y_1/Y_2, which gives rise to variations similar to those of the friction coefficients. Finally, on decreasing the final radius (i.e., increasing the extrusion ratio), the factor f assumes lower values. Although the absolute value of f does not change, as commented in Sec. 4, its normalized value diminishes since the total uniform strain increases at higher extrusion ratios. Nevertheless, the values obtained are very small.

Table 2. Evaluation of the void growth parameter, f, at variable extrusion parameters for an inner C.R.A. location.

INNER C.R.A.							
Y_1/Y_2	f	R_f/R_0	f	m_0	f	m_2	f
2.2	0.128	0.553	0.074	0.1	0.128	0.15	0.128
3.5	0.52	0.64	0.095	0.3	0.45	0.3	0.92
5	0.87	0.727	0.128	0.5	0.75	0.5	1.57

Table 3. Evaluation of the void growth parameter, f, at variable extrusion parameters for an outer C.R.A. location.

OUTER C.R.A.											
Y_2/Y_1	f	R_1/R_0	f	R_m/R_0	f	R_f/R_0	f	m_0	f	m_2	f
2.2	0.202	0.708	0.004	0.085	0.12	0.553	0.112	0.1	0.202	0.15	0.202
3.5	0.49	0.795	0.092	0.205	0.155	0.64	0.149	0.3	0.343	0.3	1.1
5	0.69	0.882	0.202	0.32	0.202	0.727	0.202	0.5	0.48	0.5	2.15

Other parameters such as the die angle, the interface radius and the mandrel radius are not included in Table 2. In the first place, on increasing the die angle (above 30°), negative hydrostatic stresses are obtained in the selected point. Therefore, there will be no tendency to void formation under these conditions. On the other hand, the same behaviour is also encountered on increasing the interface radius or on decreasing the mandrel radius. In both cases, the C.R.A. thickness increases and, as mentioned before, higher compressive stresses are attained, the

hydrostatic stress becoming negative along the interface. Accordingly, Eq. (5.1) cannot be evaluated for these three parameters.

The results for the outer location of the C.R.A. layer are included in Table 3. Again, the friction coefficients (especially with the die) provide the largest variations in the factor f. The yield stress ratio also gives rise to considerable increments in the void growth parameter.

On the other hand, on increasing the interface radius or the mandrel radius, an increase in the factor f can be noticed, since higher tensile stresses are then obtained. The final radius affects the parameter f very little: higher extrusion ratios give rise to lower factors. Finally, the die angle is not included in Table 3, for the same reason mentioned before for Table 2.

6. Discussion

A brief discussion on the method and results is presented in this section. In the first place, it should be noted that the analysis leads only to the first approach to the real process. The accuracy of the results is strongly affected by simplified assumptions on the flow. Nevertheless, the method proves to be quick and easy, and allows for an efficient analysis of the effects of the many parameters involved in the process.

The bonding along the interface does not play any role in the method. Therefore, the solution would be valid for a real flow with perfect bonding, where the velocity continuity is imposed along the material interface.

The piston force computed from Eq. (3.10) provides a value very similar to Durban's and of the same order as Blazynski and Townley's. It differs, however, from the actual industrial process because it does not take into account the discontinuities at the entry and exit sections, and other possible redundant contributions.

A comparison between the present results and finite element calculations (see [15]) under similar conditions shows that stress values of the same order are obtained (for both locations of the C.R.A.). Main difference takes place in the shear stress distribution. Here this component was shown to be independent of the radial coordinate. However, from the FE results follows a relation, showing a change from negative values at the entry to positive values at the exit. Notwithstanding this fact, the magnitude is of the same order. The sign and values of this shear stress along the contact zones (with mandrel and die) has also been checked. Finally, the qualitative effects of some of the extrusion variables (the yield stress ratio, the die angle and the thickness ratio) can also been verified by the FE results in Alcaraz [15].

7. Conclusions

An analytical approach to the stress field in the extrusion of bimetallic tubes has been performed and the influence of some relevant parameters of the process has been discussed.

The radial and normal stress components show very small dependence on the angular coordinate, what means a quasi-uniform flow. Moreover, the shear stress component does not depend on the radial coordinate (as a result of the spherical radial flow assumed in the analysis).

For an inner location of the harder material, the stress plots show that the radial stress is positive and the shear stress negative in the harder material. The signs change in case of the opposite location. Normal stresses are negative in all cases and show a decreasing trend on approaching the die exit.

A comparison of the stress levels at the exit interfacial point shows that higher stresses are obtained with higher yield stress ratios and die angles, and when the proportion of the harder material increases at an inner location. However, lower shear and radial stresses are obtained with an outer location of the harder material.

The stress values obtained at the interface are also used to assess a factor deciding on the ductile failure of the tube. It is concluded that the most influential parameters seem to be the yield stress ratio and the friction (especially with the die). Higher values of the factor are also obtained when the thickness of the harder layer decreases. Increasing the die angle, on the other hand, produces higher compressive stresses and thus helps to prevent the void growth ductile failure.

References

1. R.T. Shield, *Plastic flow in a converging conical channel*, J. Mech. and Physics of Solids, **3**, 246–258, 1955.

2. T.Z. Blazynski and S. Townley, *The methods of analysis of the process of plug drawing of bimetallic tubing applied to implosively welded composites*, Intern. J. Mech. Sciences, **20**, 785–797, 1978.

3. D. Durban, *Drawing and extrusion of composite sheets, wires and tubes*, Intern. J. Solids and Structures, **20**, 649–666, 1984.

4. A.G. Atkins and A.S. Weinstein, *The deformation of sandwich materials*, Intern. J. Mech. Sciences, **12**, 641–657, 1970.

5. C.S. Hartley, *Upper bound analysis of extrusion of axisymmetric, piecewise homogeneous tubes*, Intern. J. Mech. Sciences, **15**, 651–663, 1973.

6. H. Tokuno and K. Ikeda, *Analysis of deformation in extrusion of composite rods*, J. Materials Processing Technology, **26**, 323–335, 1991.

7. A.K. TAHERI, *Analytical study of drawing of non-bonded trimetallic strips*, Intern. J. Machine Tools Manufacturing, **33**, 71–88, 1993.

8. D.Y. YANG, Y.G. KIM and C.M. LEE, *An upper-bound solution for axisymmetric extrusion of composite rods through curved dies*, Intern. J. Machine Tools Manufacturing, **31**, 565–575, 1991.

9. B. AVITZUR, R. WU, S. TALBERT and Y.T. CHOU, *Criterion for the prevention of core fracture during extrusion of bimetal rods*, ASME J. Engng. for Industry, **104**, 293–304, 1982.

10. B. AVITZUR, R. WU, S. TALBERT and Y.T. CHOU, *Criterion for the prevention of sleeve fracture during extrusion of bimetal rods*, ASME J. Engng. for Industry, **108**, 205–212, 1986.

11. K. OSAKADA, M. LIMB and P.B. MELLOR, *Hydrostatic extrusion of composite rods with hard cores*, Intern. J. Mech. Sciences, **15**, 291–307, 1973.

12. A.T. NAGY, *Drawing of a material consisting of a hard core and a soft sleeve*, J. Mech. Working Technology, **12**, 67–77, 1985.

13. O. PAWELSKI and W. RASP, *Stresses and strains in deformation of clad metals*, [in:] Metal Forming Plasticity, H. LIPPMANN *et al.* [Eds.], Springer-Verlag, 363–377, 1979.

14. J.R. RICE and D.M. TRACEY, *On the ductile enlargement of voids in triaxial stress fields*, J. Mech. and Physics of Solids, **17**, 201–217, 1969.

15. J.L. ALCARAZ and J. GIL-SEVILLANO, *An analysis of the extrusion of bimetallic tubes by numerical simulation*, Intern. J. Mech. Sciences, **38**, 157–173, 1996.

DEPARTAMENTO DE INGENIERIA MECANICA
ESCUELA TECNICA SUPERIOR DE INGENIEROS, BILBAO, SPAIN

e-mail: impaltaj@bi.ehu.es

and

CENTRO DE ESTUDIOS E INVESTIGACIONES TECNICAS DE GUIPUZCOA (CEIT)
ESCUELA SUPERIOR DE INGENIEROS INDUSTRIALES
UNIVERSIDAD DE NAVARRA, SAN SEBASTIAN, SPAIN.

Received September 27, 1996.